Detection and formation mechanism of micro-defects in ultrafine pitch Cu–Cu direct bonding*

Zi-Yu Liu(刘子玉)[1], Jian Cai(蔡坚)[1,2,†], Qian Wang(王谦)[1], and Yu Chen(陈瑜)[1]

[1] *Institute of Microelectronics, Tsinghua University, Beijing* 100084, *China*

[2] *Tsinghua National Laboratory for Information Science and Technology, Beijing* 100084, *China*

(Received 7 May 2015; revised manuscript received 29 July 2015; published online 8 December 2015)

In this paper, Cu–Cu interconnects with ultrafine pad pitches of 6 μm, 8 μm, and 15 μm are implemented on the 12 inch wafers by a direct bonding process. Defects are not found by traditional non-destructive (NDT) c-mode scanning acoustic microscopy (c-SAM). However, cross sectional observation of bonding interfaces reveals that micro-defects such as micro seams are located at SiO_2 bonding interfaces. In order to examine the micro-defects in the ultra-fine pitch direct bonding process by the NDT technology, a novel "defect-enlarged approach" is proposed. The bonded dies are first annealed in an N_2 oven at 300 °C for a few hours and then cooled quickly in air. The c-SAM scanning images show large defects at the place where nothing can be detected by c-SAM before this treatment. Cross sectional observation of the bonding interfaces indicates that these defects consist of large size micro seams at the SiO_2 bonding interface, especially near Cu pads with an ultrafine pitch of 6 μm. However, these large defects disappear after several hours at room temperature, observed by c-SAM. It is inferred that the disappearance of these defects inspected by the "defect-enlarged approach" results from the combination of intrinsic micro seams and "weak" bonds in the silicon oxide layer. Then the underlying physical mechanism of these micro-defects is proposed, which is influenced by Cu pad surface topology and bonding models.

Keywords: nondestructive testing of materials, microscopy acoustical, surface and interface

PACS: 81.70.−q, 43.58.Ls, 73.20.Hb **DOI:** 10.1088/1674-1056/25/1/018103

1. Introduction

Cu–Cu bonding is an attractive choice for three-dimensional (3D) integration because it can achieve ultra-fine pitch, low cost, high electrical conductivity, thermal conductivity, and electromigration reliability.[1–4] Traditional thermo-compression technology needs a bonding temperature higher than 300 °C and a bonding pressure of more than 200 kPa.[3,5,6] The high bonding temperature is a challenge, for aspects such as misalignment, thermal stress and process reliability.[7] Furthermore, the high bonding pressure will introduce cracks into ultra-thin chip interconnection. In the direct bonding process, silicon oxide is pre-bonded by the hydrogen bond then the nearby Cu–Cu interfaces tightly contact each other due to the stress obtained from silicon oxide.[8–10] So neither extra bonding temperature nor pressure is exerted on the silicon wafer in the pre-bonding process. Therefore, Cu–Cu direct bonding technology is considered as one of the most promising processes used for 3D integration, and many studies of the process optimization[8,10,11] have been conducted. As the integration density increases, the bonding pitch needs to be reduced sharply and simultaneously micro-defects such as voids and seams may increase in the direct bonding process. Besides, the bonding interfaces are complicated including SiO_2–SiO_2, Cu–Cu, and SiO_2–Cu.[8] Usually the SiO_2–SiO_2 interfaces contain a bonded area, a "weak" bonded area and an un-bonded area.[12] The bonded area is defined as the area bonded with a covalent bond and the "weak" bonded area is treated as the interface with a mediate state between bonded and un-bonded. However, few studies have been performed on the detection of "weak" bonds and micro-defects of several micrometers in size especially by nondestructive testing (NDT) technologies. Defect detection in an electronic device is attracting more and more attention these days due to its practical and scientific significance.[13,14] Though a traditional c-mode scanning acoustic microscope (c-SAM) has been used to detect the defects at the wafer level,[1,8,15] there have been no data available about the micro-defects or "weak" bonds detected by NDT technologies to date because the resolution of c-SAM is limited by material and distance. Additionally "weak" bonds such as the hydrogen bond cannot be inspected by c-SAM nor other NDTs. These types of micro-defects and "weak" bonds may not be found from the cross sectional observation nor from the initial electrical tests, but they may cause long-term device reliability.

In this work, a novel approach is proposed to inspect the micro-defects with several micrometers in size after the ultrafine pitch Cu–Cu direct bonding has been implemented. Firstly, Cu–Cu interconnects with ultra-fine pitches of 6 μm, 8 μm and 15 μm are fabricated by the direct bonding process on the 12 inch wafers with a thickness of 750 μm. Defects at the bonding interfaces are not found by traditional c-SAM observation. In order to detect micro-detects such as micro seams and "weak" bonds, a "defect-enlarged approach" is applied, in which the bonded dies are annealed at 300 °C for a

*Project supported by the National Natural Science Foundation of China (Grant No. 61274111) and the National Basic Research Program of China (Grant No. 2015CB057205).

†Corresponding author. E-mail: jamescai@tsinghua.edu.cn

© 2016 Chinese Physical Society and IOP Publishing Ltd

few hours and then cooled quickly in air. The cSAM observation is subsequently carried out and the enlarged micro-detects are detected. However, enlarged micro-detects recover or disappear in the c-SAM images after several hours. Based on these observations, the defect type and formation mechanism are inferred and discussed.

2. Experiment

The process flow chart of Cu–Cu wafer level direct bonding is illustrated in Fig. 1. Figure 1(a) shows the bonding structures including the Cu bonding pad, Al routing and SiO_2 insulation layer. A pair of 12 inch wafers with a thickness of 750 μm were prepared and cleaned by the standard RCA cleaning process. An insulation layer of SiO_2 was deposited on the wafers by the plasma enhanced chemical vapor deposition (PECVD). Then aluminum with a thickness of 1 μm was evaporated and patterned as a routing layer. Thick SiO_2 passivation was formed by PECVD and patterned by the lithography. Afterwards, SiO_2 was recessed to form a damascene trench by reactive ion etch (RIE). The Ti and Cu seed layers were sputtered and followed by copper electroplating to fabricate a bonding pad. A chemical mechanical polishing (CMP) process was used to remove the copper overburden. A short-time RIE process before bonding was applied to smooth and activate the SiO_2 surface. After two wafers were dipped in the deionized water before spin drying, they were put together face to face for a few hours in air as shown in Fig. 1(b). A wafer bonder was adopted for the bonding process and all the above processes were completed in a class one cleaning room. Then pre-bonded wafers were annealed at 300 °C for 30 min in an N_2 oven. Figure 1(c) shows the top view (Z direction) of the daisy chain electrical structure after the bonding process. The bonding pad pitches of 6 μm, 8 μm and 15 μm were designed to be in the X direction and pad pitches in the Y direction were all 50 μm.

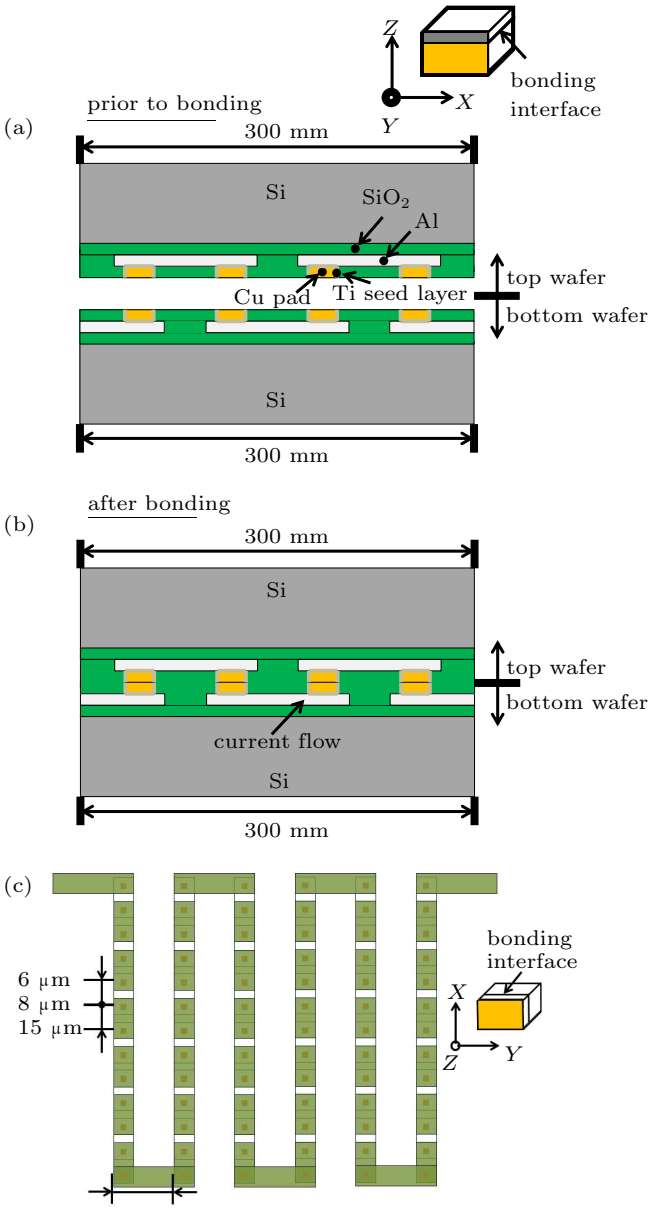


Fig. 1. (color online) Process flow illustration of Cu–Cu direct bonding (a) prior to and (b) after bonding, and (c) bonding structure design.

After bonding, bonded wafers were sliced into dies with different sizes, each of which included a daisy chain structure with all the bonding pad pitches. Then c-SAM (KSI SAM 300) was used to examine the defects such as large voids or un-bonded area. However, for the bonding interfaces with no large defects detected by c-SAM, micro seams were found in crosssectional observation by scanning electron microscopy (SEM, TESCAN LYRA3 FEG-SEM) near some Cu bonding pads, especially at the ultrafine pitch of 6 μm. Cross-sectional observation was destructive and partial so it cannot be used to detect all the micro-defects. In order to distinguish the dies with no micro-defects, a novel approach was adopted to explore the micro-defects at the bonding interfaces. It included the annealing process and quick cooling. The bonded die was annealed for a few hours in the N_2 oven and subsequently cooled quickly in air. Then c-SAM detection was used again to find out whether there are enlarged micro-defects. Besides, in order to clarify the formation mechanism of these micro-defects, the bonding interfaces were examined by SEM observation before and after the annealing process.

3. Results and discussion

Though large defects are not detected by traditional c-SAM scanning because of low theoretical resolution of traditional c-SAM, micro seams are found after cross sectional observations of different bonding pitches at some bonding interfaces. Consequently, a modified NDT approach is proposed. Ten samples are dealt with by this approach and enlarged micro-defects are found by c-SAM in three dies. Cross sectional observations are used to characterize the bonding interfaces of the enlarged micro-defects. Furthermore, enlarged micro-defects recover and disappear in the c-SAM images after several hours. Subsequently, the physical mechanism of micro-defects is inferred and discussed.

3.1. Large defects inspection and bonding interface observation

The c-SAM scanning is adopted to detect large defects such as un-bonded areas at the bonding interfaces. Owing to the high longitudinal sound velocity of silicon (8430 m/s),[16] the theoretical resolution of c-SAM imaging is relatively low. Though a high frequency ultrasonic probe can be used, the penetration depth is much lower than 750 μm, which limits the application of c-SAM in the thick bonded wafers. In order to obtain enough of a penetration depth, a 150-MHz ultrasonic probe is adopted in the c-SAM scanning process and the theoretical resolution is calculated from the following equation:

$$W = \frac{\lambda}{2 \times NA} \approx \frac{\lambda}{2} = \frac{\upsilon}{2 \times f}, \tag{1}$$

where W is the resolution, λ is the wave length, and NA is the numerical aperture of the lens. The resolution of the c-SAM is also influenced by the sample condition and transducer condition. Generally, it is equal to half the wave length. The letters υ and f represent the transmission velocity and the frequency of the ultrasonic probe, which are 8430 m/s and 150 MHz, respectively. Hence, the theoretical resolution is about 28 μm according to Eq. (1). After many samples are scanned by the 150-MHz ultrasonic probe, neither evident void nor seam is found in the bonding interface except the scribe line as shown in Fig. 2. It can be inferred that there are no defects larger than 28 μm at the interfaces.

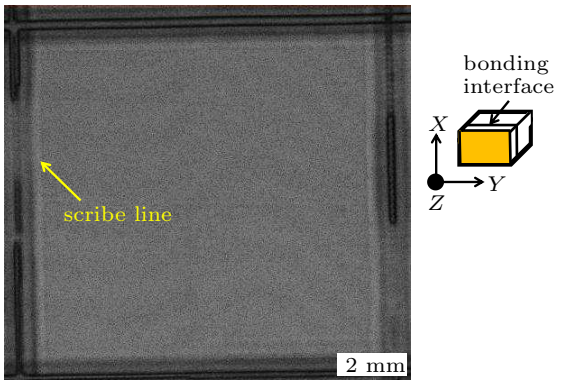


Fig. 2. (color online) C-SAM detection of large defects for sliced die after direct bonding process.

Interface microstructures of different pitches are then observed by SEM, which can be shown in Figs. 3(a)–3(c). It is obvious that Cu–Cu bonding interfaces in the Y direction are proved to have excellent adhesion without any micro-defects. However, figure 3(d) shows the micro-seams at the silicon oxide layers, which are near some bonded Cu–Cu interconnection with a pad pitch of 6 μm. However, the cross-sectional bonding interface observation is destructive and accidental so it cannot be used to distinguish micro-defects from all the dies. Then all the bonded dies are treated with the proposed NDT "defect-enlarged approach".

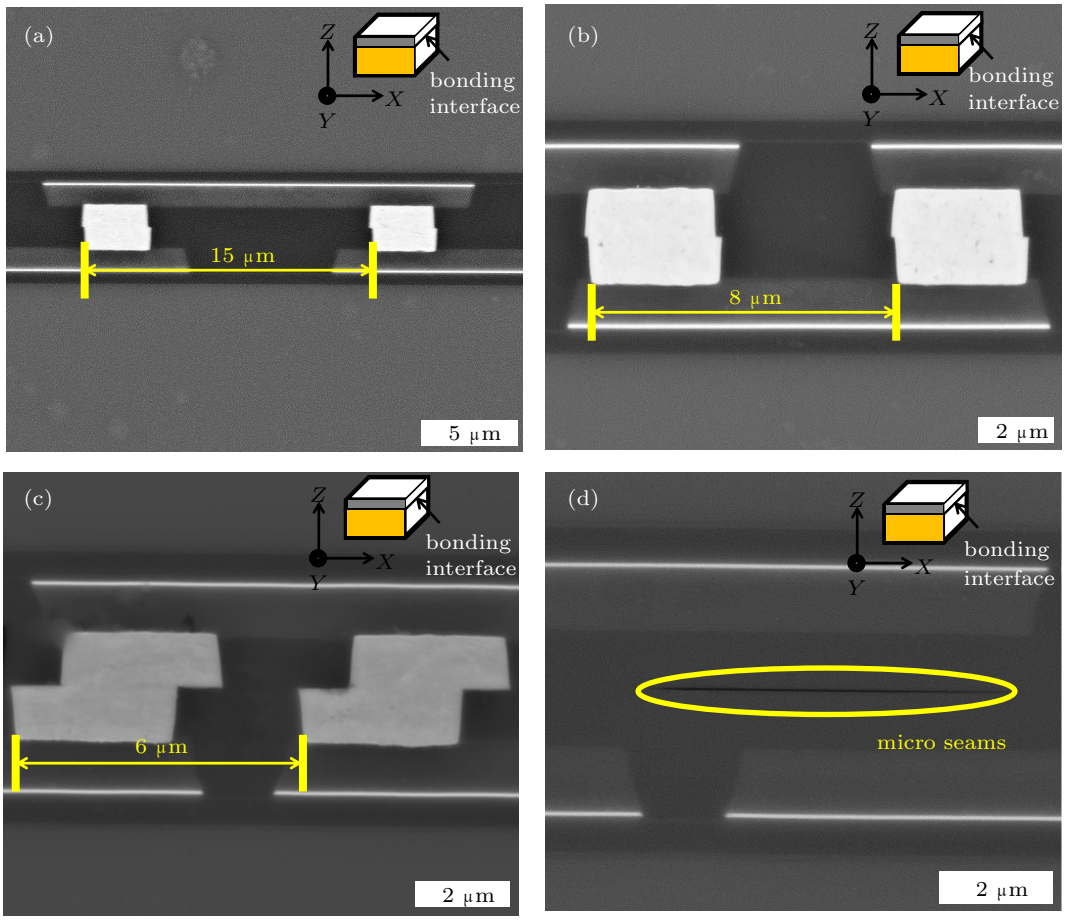


Fig. 3. Interface morphologies observation by SEM for the pitches of (a) 15 μm, (b) 8 μm, (c) 6 μm, and (d) seams near the bonded Cu pad.

3.2. Detection of micro-defects and "weak" bonds

The approach is composed of a defect-enlarging process and c-SAM scanning, so it is named the "defect-enlarged approach". First, the tested dies are annealed in an oven with N_2 atmosphere at 300 °C for a few hours. Then they are transferred out of the oven quickly and cooled in air. The c-SAM detection is used to explore micro-defects. In this approach, the annealing process is of benefit to inter-diffusion, so Cu–Cu or SiO_2–SiO_2 interfaces bonded in the direct bonding process are strengthened. However, the micro-defects such as seams or voids of the SiO_2 bonding interface will not change in the annealing process because the interior of the micro-defect is in a vacuum state. After a quick cooling process, these micro-defects will be enlarged due to thermal expansion.

Ten as-bonded samples are examined by the c-SAM images and no defect is found, which is the same as the scenario in Fig. 4(a). Afterwards they are treated by the "defect-enlarged approach". Large defects are detected in three samples, which are all similar to the case in Fig. 4(b). Additionally, most of the large defects are found in the area with a Cu pad pitch of 6 μm.

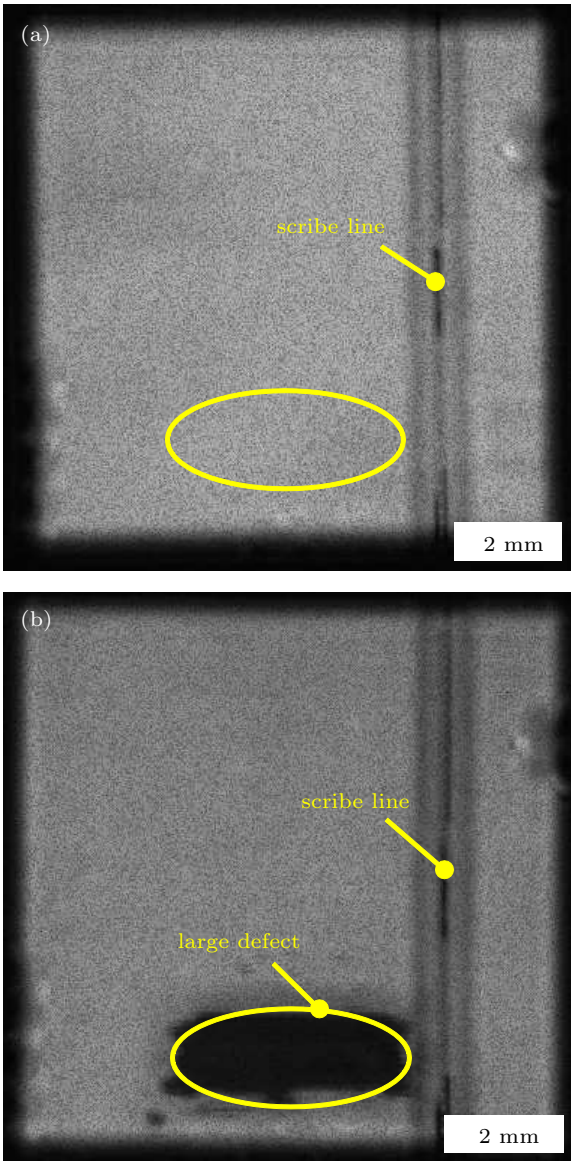


Fig. 4. (color online) The c-SAM images for sliced dies after the direct bonding process: (a) as-bonded, (b) after annealing and quick cooling.

These large defects detected by the proposed approach might originate from the combination of micro seams and "weak" bonds at the silicon oxide bonding interface. In order to identify the assumption, SEM observation is carried out to examine the interface morphologies of the large defects found by the "defect-enlarged approach". Figure 5 shows that the large defects in Fig. 4(b) consist of seams with a size of 38.2 μm along the SiO_2 bonding interface. According to the observation of Fig. 3(d), micro seams with much smaller sizes are discovered in some as-bonded samples. It can be inferred that after the treatment of the "defect-enlarged approach", micro seams are combined with cracking "weak" bonds so that they are enlarged and found by c-SAM scanning maps. The cracking process of "weak" bonds may be related to the thermal stress resulting from the coefficient of thermal expansion (CTE) mismatch between silicon oxide and Cu. So the thermal stress resulting from CTE mismatch is calculated below.

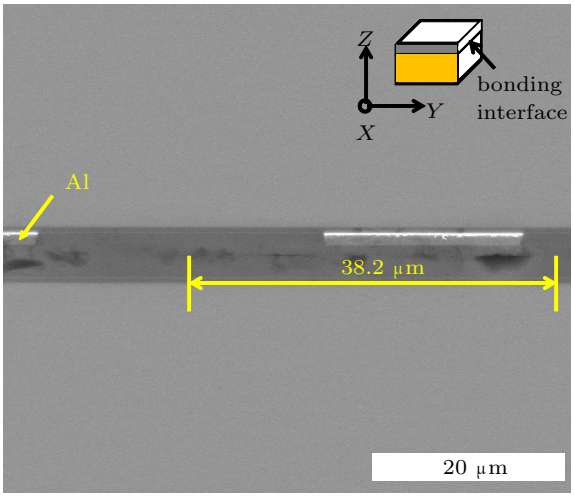


Fig. 5. (color online) SEM image of the interface morphology and microstructure after annealing and quick cooling.

The stress that the "weak" bonds experience in the annealing process and cooling process can be expressed as[17]

$$\sigma = -\frac{E_{\mathrm{Cu}}}{1-\upsilon} \times (\alpha_{\mathrm{Cu}} - \alpha_{\mathrm{SiO_2}}) \times (T_{\mathrm{a}} - T_{\mathrm{r}}), \tag{2}$$

where σ is the stress; E_{Cu} is the elastic modulus of Cu (129.8 GPa); υ is the Poisson ratio (0.324);[17] α_{Cu} and $\alpha_{\mathrm{SiO_2}}$ are the CTEs of Cu and SiO_2, which are 17×10^{-6} °C^{-1} [18] and $0.6 \pm 0.2 \times 10^{-6}$ °C^{-1},[19] respectively; T_{a} and T_{r} are the annealing temperature and room temperature, which are 300 °C and 25 °C, respectively. So the tensile stress exerted on the SiO_2 (the compression stress on the Cu) is about 866 MPa.

This value is much higher than the strength of a "weak" bond, which is likely to be composed of hydrogen bonds at the SiO_2 bonding interfaces. After the cracking of "weak" bonds, the interfaces of the seams are in a high vacuum state. Owing to the pressure difference between the atmosphere on the silicon and the high vacuum in the seam, "weak" bonds may be compressed together after some time. Owing to the intermolecular force of hydrogen bonds, a continuous adhesive SiO_2 layer forms again. Simultaneously, large defects found by c-SAM are decomposed into micro seams and "weak" bonds. If this assumption was corrected, large defects detected by the "defect-enlarged approach" would disappear after several hours. Therefore, c-SAM inspection is carried out to observe the enlarged defects after the annealing and quick cooling process.

3.3. Recovery of the "weak" bonds

As expected by the above assumption, after several hours, which depends on the size of defect, large defects disappear, and no defect is observed in the c-SAM scanning images. The recovery process is shown in Fig. 6. Figure 6(a) shows the bonding quality of the dies as-bonded. Figure 6(b) demonstrates a large defect found by c-SAM immediately after the annealing and quick cooling process. After several hours, the large defects gradually disappear as shown in Figs. 6(c) to 6(f). In order to explore the cause of the large defect recovery process, interface morphologies after the treatment by the "defect-enlarged approach" are observed by SEM. Figure 7(a) shows the seams with lengths of tens of micrometers immediately after annealing and quick cooling, which are larger than the resolution of c-SAM scanning. This is also viewed and evidenced in Fig. 5. However, after 182 hours the lengths of seams are reduced to several micrometers as shown in Fig. 7(b), which is much smaller than c-SAM detection resolution.

Based on the recovery process of defects, it is concluded that large defects found by the "defect-enlarged approach" result from the combination of micro seams and cracking "weak" bonds. Then the recovery process of "weak" bonds is due to the pressure difference between the atmosphere on the silicon and the high vacuum in the seam. Though micro-defects can be discovered in this work, the underlying physical formation mechanism of the seams in the interfaces needs to be investigated, which is beneficial for controlling the bonding process.

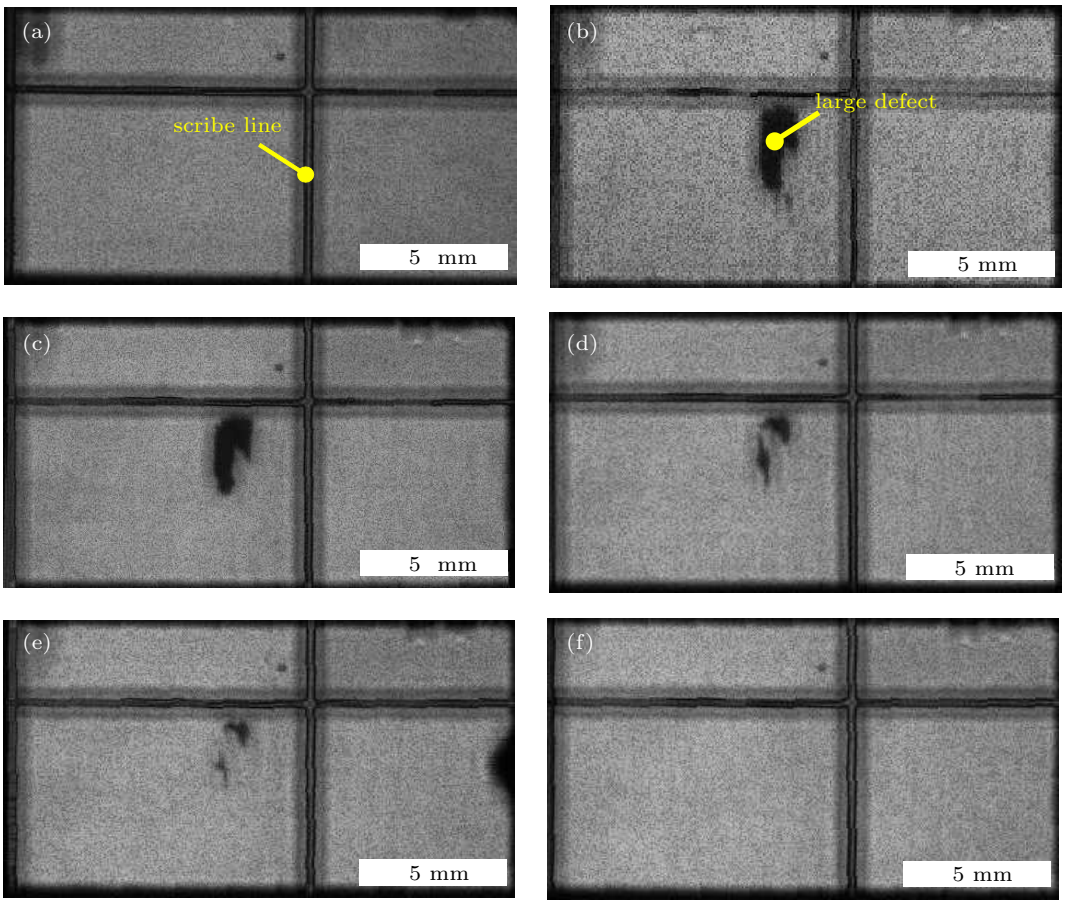


Fig. 6. (color online) Defect recovery processes observed (a) before annealing and cooling, (b) immediately after annealing and cooling, (c) after 38 hours, (d) after 64 hours, (e) after 84 hours, and (f) after 182 hours.

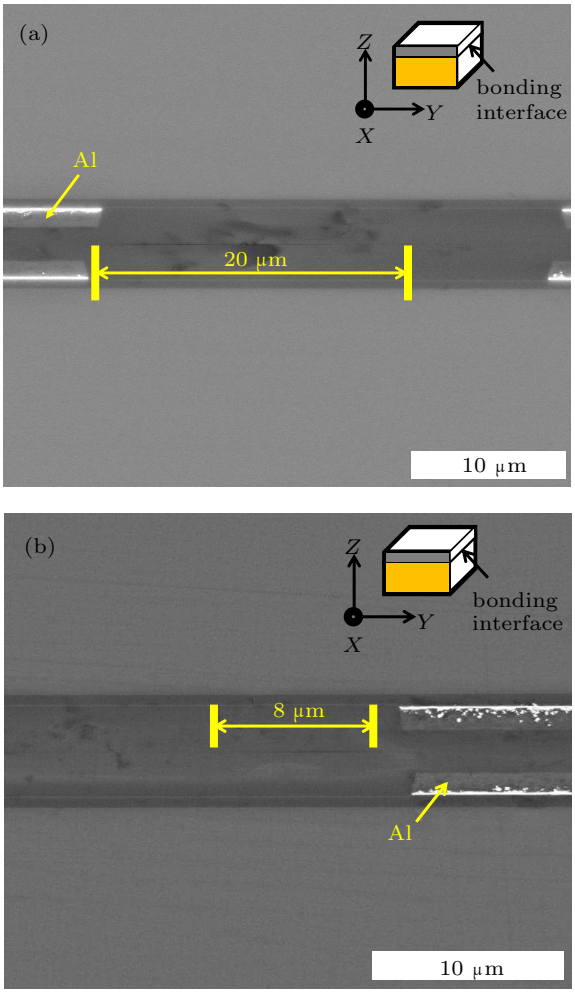


Fig. 7. (color online) Interface morphologies of the cross section (a) after annealing and quick cooling and (b) 182 hours later.

The underlying formation mechanism of the micro-defects is concerned with Cu pad surface topology and the bonding model, which is illustrated in Fig. 8. Owing to a possible non-homogeneity in the CMP process, three kinds of Cu surface topologies can be developed, such as copper in protrusion, copper in dishing, and flat surfaces, as respectively shown in Figs. 8(a), 8(c), and 8(e). Consequently three possible bonding models as depicted in Figs. 8(b), 8(d), and 8(f) are used to illustrate the bonding process. When Cu in protrusion is bonded together as depicted in Fig. 8(b), micro seams of SiO_2 may be formed around the Cu pad because the height variation between Cu and SiO_2 cannot be compensated for by Cu plastic deformation. If the bonding Cu pad pitch is ultrafine, the spaces between these micro seams are so narrow that merely "weak" bonds like the hydrogen bond are used to link the SiO_2, which further reduces Cu plastic deformation. These assumptions indicate that there may be more micro-defects around the ultrafine Cu pad pitch, which is identified by the results in this work that there are more micro-defects around the Cu pad with a pitch of 6 μm. More micro-defects in the ultrafine pitch bonding process may also result from the reduced homogeneity of the Cu surface and SiO_2 surface after the CMP process because of the high Cu pad density. Additionally, the shapes of micro seams around Cu pads are various, which are presented as red ellipses in Fig. 9. Continuous bonding interfaces as shown in Figs. 3(a)–3(c) can be examined if position "a" in Fig. 9 is dealt with by polishing the cross section. If the interface at position "b" in Fig. 9 has a polished cross-section, micro seams around the Cu pad as shown in Fig. 3(d) can be observed. However, these micro seams are so small that they cannot be detected by traditional c-SAM, nor the "weak" bonds. When these micro-defects experience the annealing and quick cooling process, large defects at bonded interfaces are easily found by the c-SAM due to the combination of micro seams and cracked "weak" bonds. As Cu pads are flat or in dishing, the bonding models are shown respectively in Figs. 8(d) and 8(f). After bonding, they may be bonded together due to thermal expansion or they are cracked, which can be tested by electrical tests.

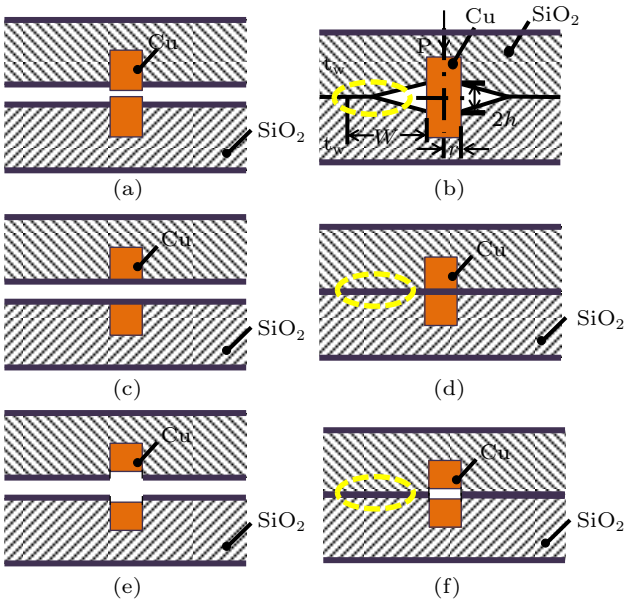


Fig. 8. (color online) Schematic diagrams of surface topology after CMP process of (a) copper in protrusion, (c) flat surface, and (e) copper in dishing. Possible bonding models at the interface of (b) copper in protrusion, (d) flat surface, and (f) copper in dishing.

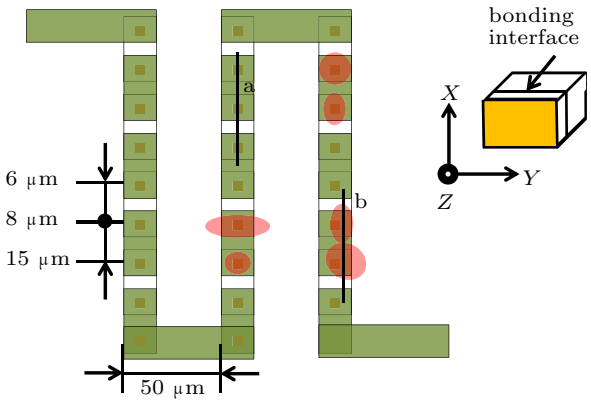


Fig. 9. Possible cross sectional interface after treatment by "defect-enlarged approach".

4. Conclusions

In this study, the Cu–Cu interconnects with the ultrafine pitches of 6 μm, 8 μm, and 15 μm are implemented by the direct bonding process. A novel effective NDT technology named the "defect-enlarged approach" is proposed to detect micro-defects. It includes an annealing process in an N_2 oven and a quick cooling process in air. After the proposed approach is applied, large defects composed of micro seams and "weak" bonds are found where no defect is detected by traditional c-SAM; these defects disappear in c-SAM images after several hours because "weak" bonds are re-bonded due to the air pressure difference. The underlying physical mechanism originates from the non-homogeneity of Cu surface roughness in the CMP process. In conclusion, the "defect-enlarged approach" is a promising NDT technology for examining the micro-defects in a direct bonding process, and is especially effective in a bonding process with an ultrafine pad pitch of 6 μm. Furthermore, it is significantly important to optimize the CMP process for different bonding processes with different Cu pad pitches, and design rules of Cu pads with a pitch of 6 μm may also be different from those with other pad pitches.

Acknowledgment

The authors appreciate Mr. Long Zhang from the Institute of Microelectronics, Tsinghua University for his help with cross section preparation.

References

[1] Tan C S, Peng L, Fan J, Li H Y and Gao S 2012 *IEEE Trans. Device Mater. Rel.* **12** 194
[2] Chen K N, Fan A, Tan C S, Reif R and Wen C Y 2002 *Appl. Phys. Lett.* **81** 3774
[3] Peng L, Zhang L, Fan J, Li H Y, Lim D F and Tan C S 2012 *IEEE Electron Device Lett.* **33** 1747
[4] Qian L B, Zhu Z M and Yang Y T 2012 *Acta Phys. Sin.* **61** 68001 (in Chinese)
[5] Sakai T, Imaizumi N and Miyajima T 2012 *2nd IEEE CPMT Symposium Japan*, December 10–12, 2012, Kyoto, Japan, p. 1
[6] Chen K N, Fan A, Tan C S and Reif R 2003 *J. Electron. Mater.* **32** 1371
[7] Chen K N, Chang S M, Fan A, Tan C S, Shen L C and Reif R 2005 *Appl. Phys. Lett.* **87** 31909
[8] Cioccio L D, Gueguen P, Taibi R, Landru D, Gaudin G, Chappaz C, Rieutord F, Crecy F D, Radu I, Chapelon L L and Clavelier L 2011 *J. Eelectrochem. Soc.* **158** P81
[9] Enquist P 2007 *Mater. Res. Soc. Symp. Proc.* **970** 13
[10] Enquist P, Fountain G, Petteway C, Hollingsworth A and Grady H 2009 *IEEE International Conference on 3D Systems Integration Conference*, September 28, 2009, San Francisco, USA, p. 374
[11] Gueguen P, Cioccio L D, Gergaud P, Rivoire M, Scevola D, Zussy M, Charvet A M, Bally L, Lafond D and Clavelier L 2009 *J. Eelectrochem. Soc.* **10** H772
[12] Twerdowski E, Wannemacher R, Schindler A, Razek N and Grill W 2005 *Proc. SPIE* **5768** 204
[13] Tanaka S, Akai T, Takemoto M, Hatsukade Y, Ohtani T, Ikeda Y and Suzuki S 2010 *Chin. Phys. Lett.* **27** 88503
[14] Chen Z J, Zheng J, Zhang S Y, Mi X B and Zheng K 2012 *Chin. Phys. B* **19** 118104
[15] Gueguen P, Cioccio L D, Gonchond J P, Gergaud P, Rivoire M, Scevola D, Zussy M, Lafond D and Clavelier L 2009 *Mater. Res. Soc. Symp. Proc.* **1112** 81
[16] http://en.wikipedia.org/wiki/Speeds_of_sound_of_the_elements_(data_page)
[17] Zhang J M and Xu K W 2002 *Acta Phys. Sin.* **51** 2562 (in Chinese)
[18] Murarka S P 1997 *Mater. Sci. Eng. R* **19** 87
[19] Ambrée P, Kreller F, Wolf R and Wandel K 1993 *J. Vac. Sci. Technol. B* **11** 614